A COMPACT TUNABLE DUAL-STOP-BAND FILTER BASED ON DMS AND DGS

Ming Zhong Lin[*]**, Qiu Yi Wu, Zi Han Wu, and Xiao Wei Shi**

National Key Laboratory of Science and Technology on Antennas and Microwaves, Xidian University, Xi'an, Shanxi 710071, China

Abstract—In this paper, a compact tunable dual-stop-band filter is proposed. The proposed filter is based on the combination of double H-shaped defected ground structure (HDGS) and E-shaped defected microstrip structure (EDMS). The loaded HDGS/EDMS varactor diode is introduced to realize the tunable dual-stop-band filter. The equivalent-circuit models and theoretical analysis of the proposed structure are presented; also its performance evaluation is compared with traditional structure. The proposed filter has the characteristic of two independently adjustable stopbands and wide tuning range. EDMS also shows size reduction up to 38% compared with the T-shaped defected microstrip structure. The measured performance of the tunable dual-stop-band filter agrees well with the simulation results.

1. INTRODUCTION

With the rapid development in wireless technology and modern communication systems, bandstop filters are widely used to attenuate the interfering signal in the systems. These systems in crowded and dynamic spectral environments will increasingly rely on tunable stopband filters [1]. To filter out several interfering signals in these systems, independently tunable dual-stop-band filter is being increasingly adopted in the industries. Conventionally, most of works are about ordinary bandstop filters [2, 3], little of which involve with tunable dual-stop-band filters [4]. In [5–9], tunable one stop-band filters are proposed based on varactor loaded split ring resonators, RF-MEMS metamaterials and DGS respectively. In [10–12], filters with dual stopband are based on tri-section stepped-impedance resonators, dual-mode loop resonator and microstrip open-loop resonators.

Microstrip lines with patterned ground such as slots or/and etched patches (DGS) and defected microstrip structure (DMS) have attracted a lot of attention due to their unique characteristics. DMS has the advantages of a prominent stopband and slow-wave effect. DGS exhibit advantages such as ease of fabrication and compatibility with monolithic microwave integrated circuits [13]. Various defected structures have been proposed and applied for rejection filters and for other optimization of microwave devices.

In this paper, the loaded HDGS/EDMS varactor diode is introduced to realize the tunable dual-stop-band filter. The proposed filter has the characteristic of two independently adjustable stopbands, wide tuning range and significant size reduction compared with the conventional structure in [14].

2. ANALYSIS OF HDGS AND EDMS

2.1. Analysis and Outline of the HDGS Resonator

DGS has its unique characteristics including sharp transition knee, compact size and no unnecessary harmonics in wide frequency range. So the DGS and improved DGS have been applied to design filters in many occasions. In this paper, a novel tunable DGS is presented. The combination of double HDGS will produce the first stopband of the proposed filter.

The proposed HDGS can be equivalent to the parallel RLC resonance circuit, as shown in Fig. 3(b), which is based on the parameters extracted from the equivalent-circuit mode [15]. Due to the low confinement of electromagnetic field around the etched patch (from Fig. 1(b)), the coupling between the central ground line and the edge of etched patch is neglected, and the value of diode corresponding to the coupling is very small. When C_1 is very small, the node $A1$ and $A2$ are equivalent to open circuit and the circuit (Fig. 3(b)) will work as a low-pass filter. The following analysis is about the HDGS with varactor diode.

The equivalent circuit of the HDGS with varactor diode is shown in Fig. 3(a). $C_{j2} = 2\,\mathrm{pF}$ is the varactor diode and C_1 represents the mutual coupling between the etched patch and the ground. The circuit parameters can be extracted from the following formula [16]:

$$C = \frac{\omega_c}{2Z_0 \left(\omega_0^2 - \omega_c^2\right)} \tag{1}$$

$$L = \frac{1}{4\pi^2 f_0^2 C} \tag{2}$$

$$R = \frac{2Z_0}{\sqrt{\frac{1}{|S_{11}(\omega_0)|^2} - \left(2Z_0\left(\omega_0 C - \frac{1}{\omega_0 L}\right)\right)^2 - 1}} \qquad (3)$$

where ω_0 is the angular resonant frequency, ω_c is the 3-dB cutoff angular frequency, Z_0 is the characteristic impedance of the microstrip line and S_{11} is the reflection coefficient at resonant frequency. By applying the simulation results shown in Fig. 2(b) to Equations (1)–(3), the equivalent circuit parameters of HDGS with diode are obtained as: $L = 3.004\,\text{nH}$, $C = 2.1023\,\text{pF}$ and $R = 1149\,\Omega$. A schematic based on the equivalent circuit shown in Fig. 3(a) is created in the Advanced Design System 2011 (ADS 2011). As shown in Fig. 4(a), the equivalent-circuit simulation results are in good agreement with full-wave simulation results in HFSS 13.0. Moreover, $C_1 = 0.1023\,\text{pF}$ is obtained and the equivalent-circuit model of HDGS without the diodes
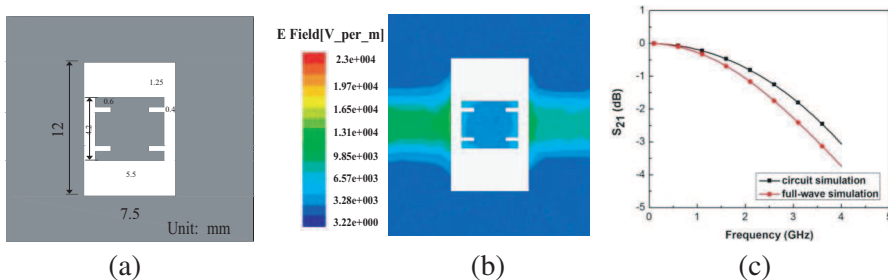
Figure 1. (a) Geometry of the HDGS without varactor. (b) Distributed current of the HDGS. (c) S_{21}-parameters of circuit simulation and full-wave simulation without diode.
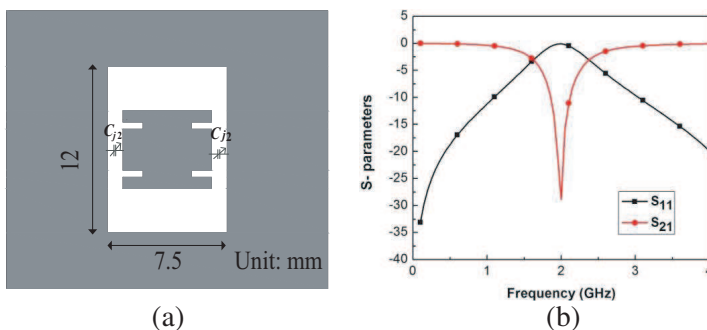
Figure 2. (a) Geometries of the HDGS with $C_{j2} = 2.0\,\text{pF}$. (b) S_{21}-parameters of the HDGS with $C_{j2} = 2.0\,\text{pF}$.
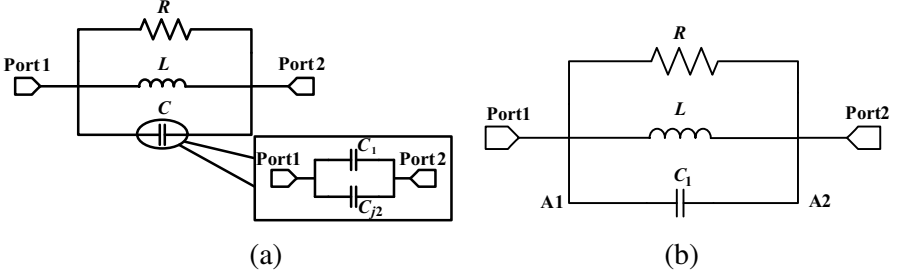
Figure 3. Equivalent circuit mode of the proposed HDGS. (a) With capacitors across the gap. (b) Without diode.
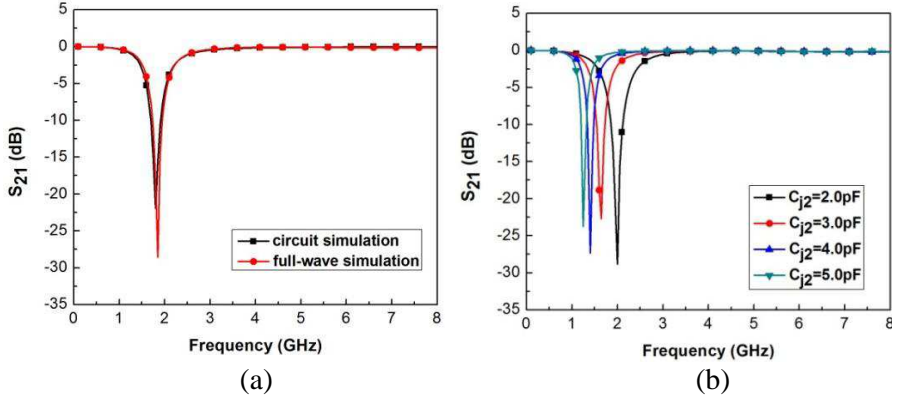
Figure 4. S_{21}-parameters of HDGS with varactor diode. (a) $C_{j2} = 2.0 \, \text{pF}$. (b) C_{j2} from $2 \, \text{pF}$ to $5 \, \text{pF}$.

is created in ADS 2011. Fig. 1(c) shows that the circuit-simulation results and full-wave simulation results of HDGS without capacitors have the same trends. This further indicates that the analysis above is credible.

Finally, as shown in Fig. 4(b), HDGS with varactor diode from $2 \, \text{pF}$ to $5 \, \text{pF}$ has a resonant frequency varying from $1.2 \, \text{GHz}$ to $2.0 \, \text{GHz}$.

2.2. Analysis and Outline of the EDMS Resonator

Although there are several methods to realize a stopband, the E-shaped defected microstrip structure appears more attractive for the stop-band filter design. The defected structure will disturb the shield current distribution in the microstrip line by adding inductances and capacitances to the main line. This effect on microstrip line is related

to slow-wave factors. The slow-wave microstrip line can improve the phase constant β of the electromagnetic wave conducted in the microstrip. Then the unit electrical length will decrease with the increase of phase constant β. So the EDMS is introduced to miniaturize the proposed filter.

Figure 5(a) shows the geometries of T-shaped DMS used in [14] and the EDMS proposed in this paper. As shown in the Fig. 5(b), the EDMS can produce a more sharper transition knee than the T-shaped DMS. The occupying area of T-shaped DMS is $23.52\,\text{mm}^2$ but the occupying area for the proposed EDMS is only $14.4\,\text{mm}^2$.

A stopband DMS with its parallel resonance equivalent circuit is reported in [17]. The DMS behaves as a lumped inductor with
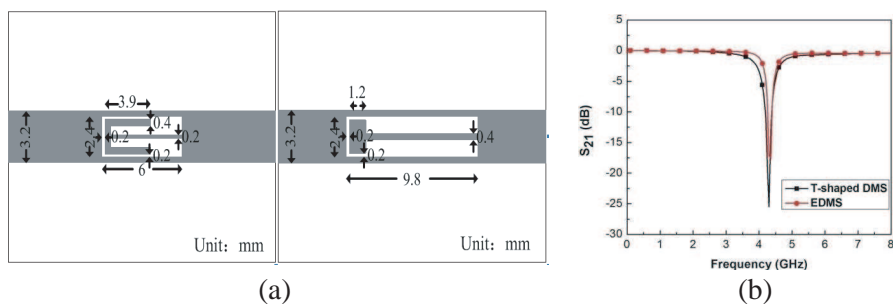
Figure 5. (a) Geometries of TDMS and the EDMS. (b) Simulated results of TDMS and the EDMS.
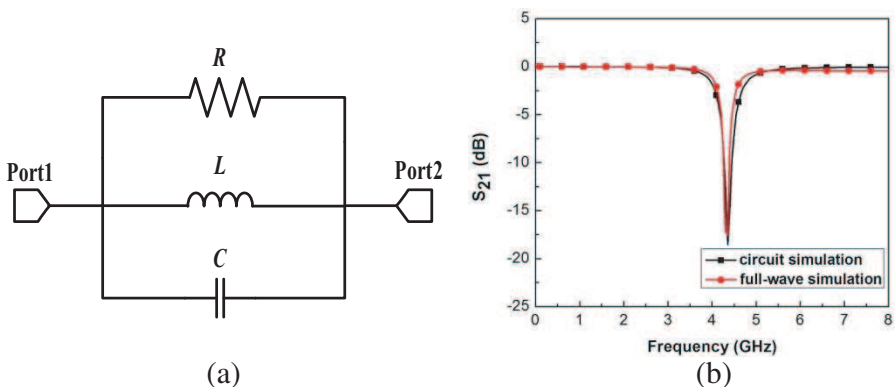
Figure 6. (a) Equivalent circuit of the EDMS. (b) Comparison of S_{21} between the full-wave simulation and circuit simulation of the EDMS.

frequency below the parallel resonance frequency and it works as a capacitor with frequency above the parallel resonance frequency. When frequency is equal to the parallel resonance frequency, the DMS can work as a stopband filter. Fig. 6(a) shows the equivalent circuit of EDMS (shown in Fig. 5(a)). The circuit parameters are $L = 0.4045\,\mathrm{nH}$, $C = 3.0921\,\mathrm{pF}$ and $R = 800\,\Omega$ (derived from the Equations (1)–(3)). Fig. 6(b) shows that the circuit simulation result is in good agreement with the full-wave simulation result.

As shown in Fig. 7, the resonance frequency of the EDMS is dependent on the structure parameters. The dimensions of E-shaped arm length (L, $L1$, $L2$) and gap (G) between EDMS and main microstrip line are the parameters changing the resonance frequency.

In Fig. 7(a), the simulated transfer characteristics for the EDMS
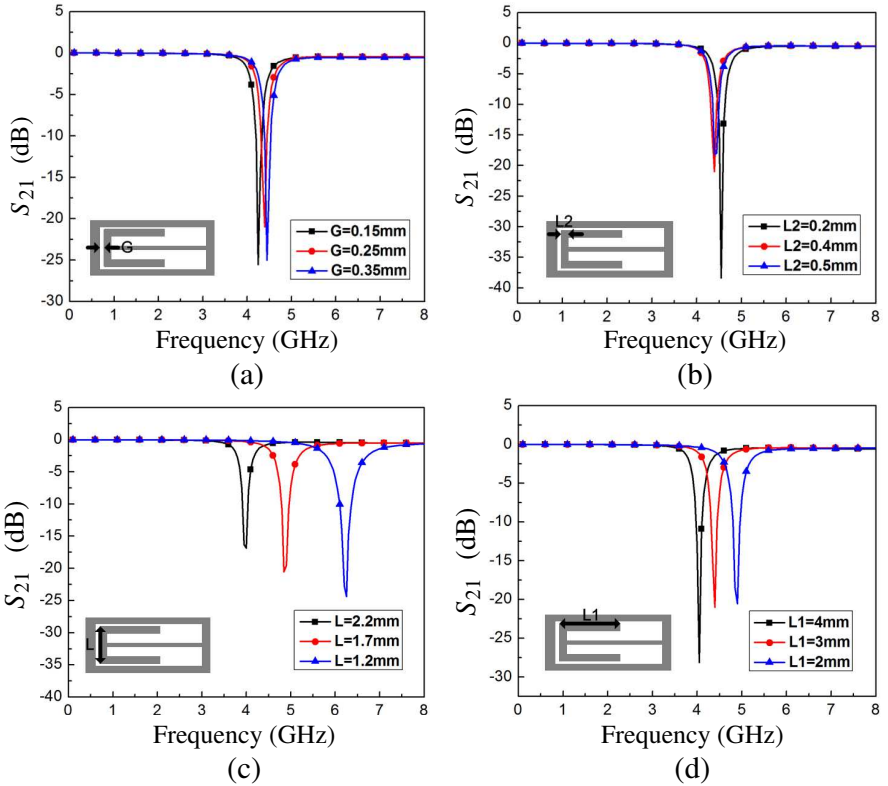
Figure 7. Transfer characteristic for the parameters (a) gap G, (b) width $L2$, (c) length L, (d) length $L1$.

are plotted as a function of gap (G). As the gap increases, the resonance frequency increase with the rejection bandwith constant. The equivalent capacitance and the equivalent inductance decreases with the gap (G) growing. The simulated results for various width $(L2)$ are shown in Fig. 7(b). Because of the neglected capacitance caused by the reduce of width $(L2)$, as can be seen in the Fig. 7(b), the resonance frequency is almost constant with the variation of width $(L2)$. Fig. 7(c) and Fig. 7(d) describe the transfer characteristics for various L and $L1$. The resonance frequency decrease and the rejection bandwidth stay constant with the increase of $L1$. The resonance frequency and rejection bandwith decrease with the value of L growing. These are resulted from the increase of capacitance and inductance as L and $L1$ increase.
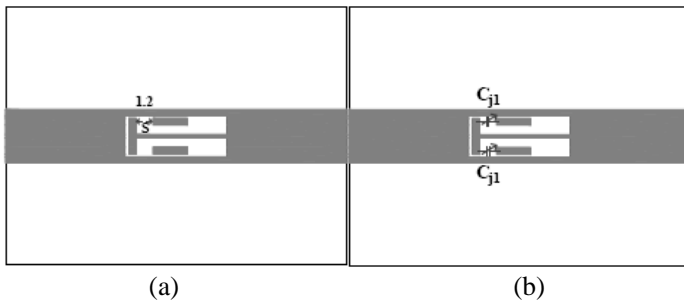
Figure 8. Layout of the two types of EDMS. (a) With gap $S = 1.2$ mm. (b) With diode across the gap.
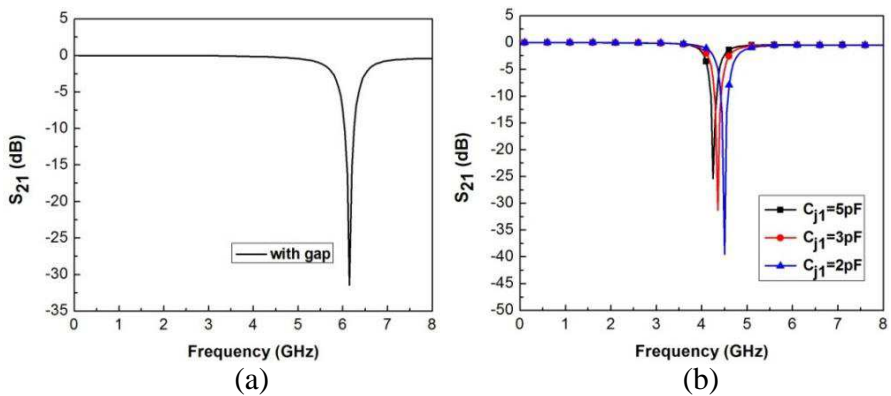
Figure 9. Simulated results of EDMS. (a) With gap $S = 1.2$ mm. (b) With varactor diode across the gap.

The diode is inserted into the E-shaped arms to change its electrical length, and the capacitance/inductance caused by the arms will change with the different electrical length. It is difficult to combine the diode with the E-shaped arm (L), as the arm (L) is not long enough and the rejection bandwith changed with the diversification of the arm (L). But the E-shaped arm ($L1$) are ease of varactor integration to realize a tunable resonance frequency.

Figure 8 shows the dimension of EDMS with gap and diode across the gap. As shown in Fig. 9, the structure with gap has a resonant frequency of 6.1 GHz, whereas the structure with varactor diode from 5 pF to 2 pF shows a resonant frequency varies from 4.2 GHz to 4.5 GHz.

2.3. Configuration of the Proposed Filter

In the view of the basis of aforementioned analysis, the proposed filter can be designed in this section. The layout of the proposed compact tunable dual-stop-band filter is shown in Fig. 10. When the bias circuit is joined, the capacitor C_{bypass} chosen as 5 pF can work as the DC-blocked capacitor. The substrate is utilized by *Rogers RT/Duroid* 5880 ($\varepsilon_r = 2.2$, $h = 1$ mm). C_{j1} and C_{j2} are the BB857 varactor from the Infineon Corporation.

(a)   (b)
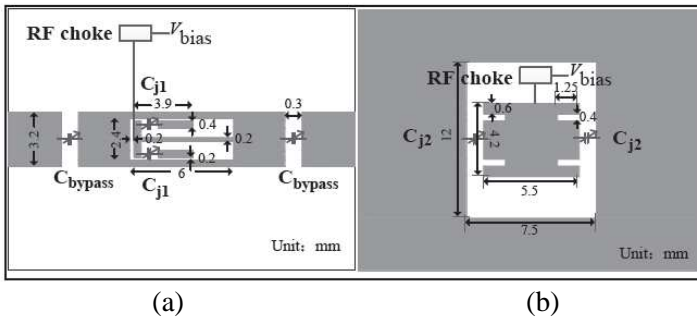
Figure 10. Layout of proposed with varactor diode. (a) Top view. (b) Bottom view.

2.4. Coupling between the HDGS and the EDMS

The C_{bypass} contribute little to the mutual coupling of the HDGS and EDMS, and it only works as a DC-block in bias circuit. When it comes to the mutual coupling, the C_{bypass} could be ignored. First of all, the filter which merely has the HDGS is build and the simulated results
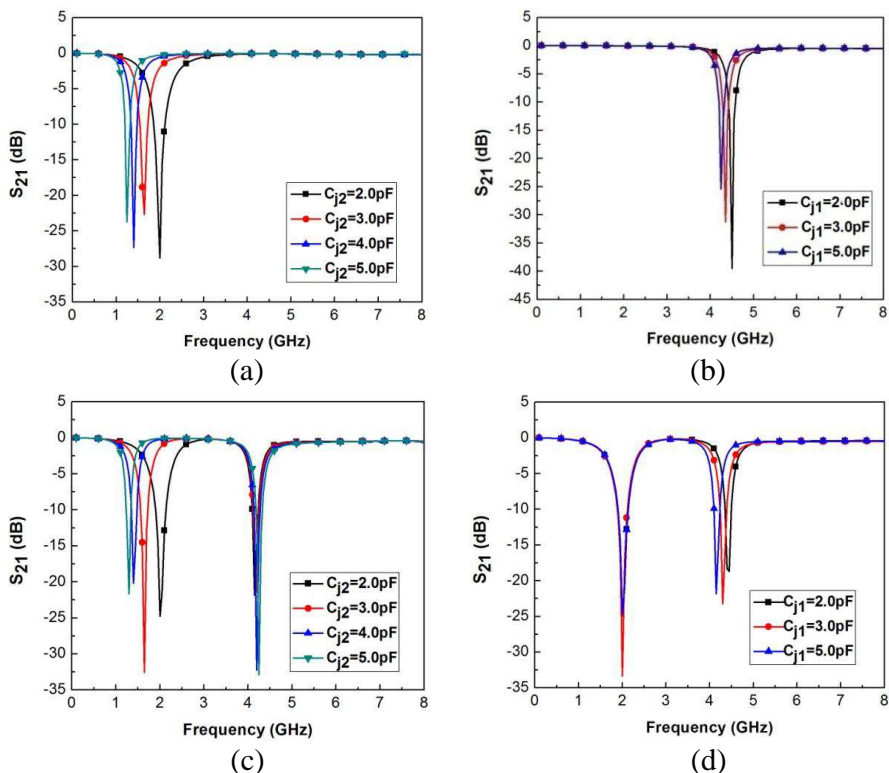
Figure 11. The simulated results of the proposed filter. (a) Without EDMS. (b) Without HDGS (c). (d) Simulated results of proposed filter DC-block capacitor.

are presented in Fig. 11(a). As shown in Fig. 11(a) and Fig. 11(c), the tuning range of the individual structures is the same with the one of the first stopband of proposed filter (from 1.2 GHz to 2.0 GHz). So the EDMS has little influence on the HDGS. Then the individual EDMS is used to create the filter and the simulation results are shown in Fig. 11(b). As shown in the Fig. 11(b) and Fig. 11(d), the adjustment range of the proposed filter and the individual EDMS are almost the same (from 4.2 GHz to 4.5 GHz). Hence, it can conclude that the HDGS has little effect on the EDMS. Finally, as shown in the Figs. 11(c) and (d), when the first stopband varies from 1.2 GHz to 2.0 GHz, the second stopband keeps invariant. Moreover, the first stopband stays constant when the second stopband varies. This phenomenon further confirms that the mutual coupling is negligible.

3. DESIGN OF TUNABLE DUAL-STOP-BAND FILTER AND MEASUREMENT

By adopting the HDGS and EDMS design concepts described in Section 2, the proposed filter is then implemented as follows.

In order to verify the influence of blocking capacitor C_{bypass} on the transfer characteristics, a co-simulation based on HFSS 13.0 and ADS 2011 is adopted. Fig. 12 shows the co-simulation results.

As shown in Fig. 12, C_{bypass} has very little influence on the performance of the the proposed filter and the results agree well with the prediction based on the analysis above.

To validate the design and analysis above, the proposed filter is fabricated and its photograph is presented in Fig. 13.

The vector network analyzer Agilent N5230A is utilized to measure
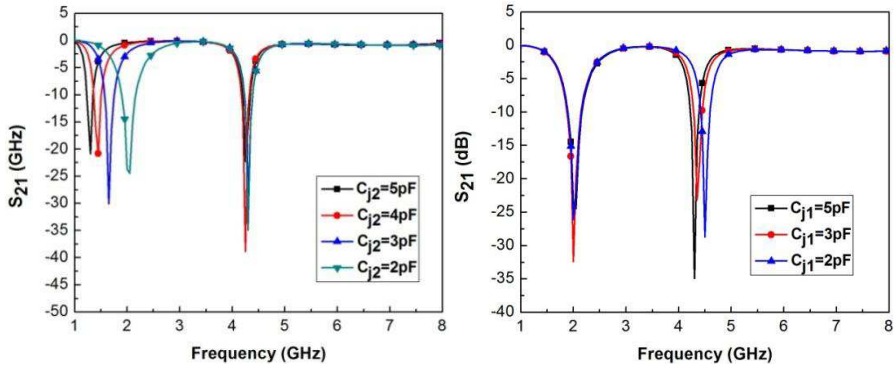
Figure 12. Results of the co-simulation.
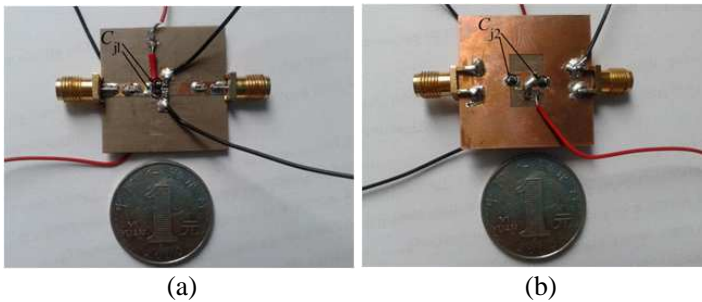
Figure 13. Photograph of the fabricated tunable dual-stop-band filter. (a) Top view. (b) Bottom view.

the transfer characteristic of the fabricated filter. From Fig. 14, it is found that the tuning range of the first stopband is from 1.2 GHz to 2.1 GHz with S_{21} better than -15 dB and the second stopband could be tuned from 4.25 GHz to 4.55 GHz with S_{21} better than -10 dB. However, the measured second stopband of the proposed filter is not as good as prediction, which may be due to the poor performance of varactor at high frequency and manufactory accuracy. Table 1 shows the measurement of the fabricated tunable dual-stop-band filter. Table 2 presents the comparison of the previous dual-stop-band filter and proposed filter.

The simulated and measured results of the proposed filter are shown in Fig. 12 and Fig. 14. Good agreements are obtained. The simulated tuning ranges are from 1.2 GHz to 2.1 GHz and from 4.25 GHz to 4.55 GHz with S_{21} better than -20 dB. The measured tuning ranges are the same with the simulated one. But the simulated S_{21} is better than the measured one. Both simulated and measured results show that good band-edge selectivity is achieved.
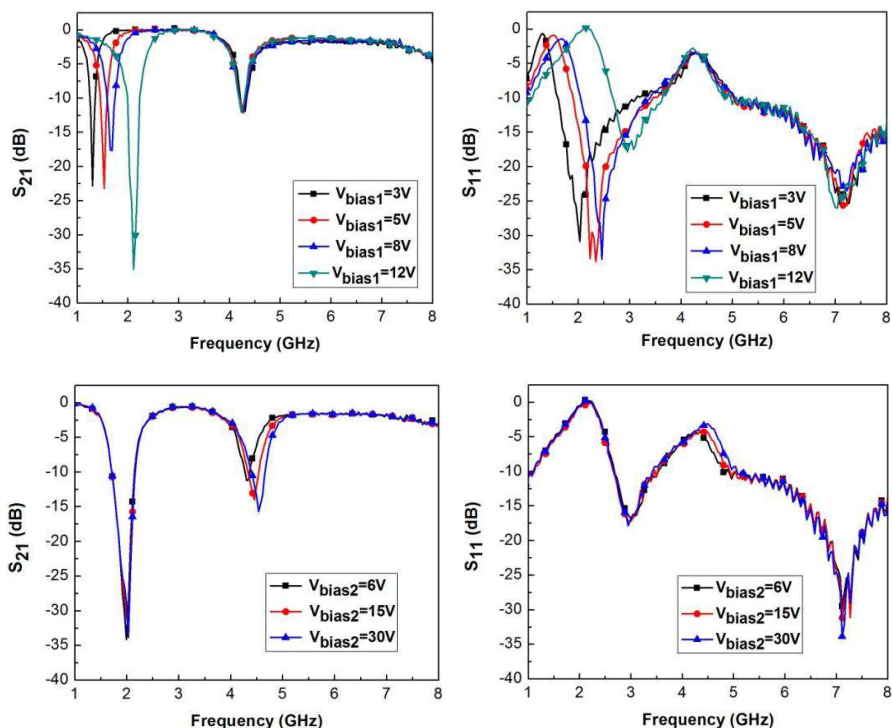
Figure 14. Measured results.

Table 1. Measurement of tunable dual-stop-band filter.

$V_{\text{bias2}} = 6\,\text{V}$			$V_{\text{bias1}} = 12\,\text{V}$		
V_{bias1} (V)	f_1 (GHz)	f_2 (GHz)	V_{bias2} (V)	f_1 (GHz)	f_2 (GHz)
3	1.2	4.2	6	2.0	4.25
5	1.5	4.2	15	2.0	4.50
8	1.6	4.2	30	2.0	4.55
12	2.1	4.2	—	—	—

* "—" represents there is no data, because of the maximum tuning range of the second stopband.

Table 2. Comparison between the previous dual-stop-band filter and proposed filter.

Structure	Tunable	Size (λ_g^2)	Structure	Tunable	Size (λ_g^2)
Proposed	Yes	0.191	[11]	No	0.344
[10]	No	0.213	[12]	No	0.427

4. CONCLUSION

In this paper, a compact tunable dual-stop-band filter based on EDMS and HDGS is proposed. The proposed filter has the characteristics of independently adjustable, compactness and wide tuning range. It is shown that the two tunable stop-bands can be designed independently. The individual equivalent circuits and theoretical analysis of the HDGS and EDMS are presented. The full-wave simulation, circuit simulation and co-simulation of HFSS and ADS 2011 are taken to verify the correctness of analysis. Based on the detailed analysis above, the proposed filter is designed and fabricated and measured results agree well with the simulation results. The first stopband has 54.5% tuning range with S_{21} better than $-15\,\text{dB}$ and the second stopband has 6.81% tuning range (from 4.25 GHz to 4.55 GHz) with S_{21} better than $-10\,\text{dB}$.

REFERENCES

1. Hunter, I. C. and J. D. Rhodes, "Electronically tunable microwave bandstop filters," *IEEE Trans. Microw. Theory Tech.*, Vol. 30, No. 9, 1361–1367, Sep. 1982.

2. Zhou, L. H., H. Tang, J. X. Chen, and Z. H. Bao, "Tunable filtering balun with enhanced stopband rejection," *Electron. Lett.,* Vol. 48, No. 14, 845–847, Jul. 2012.

3. Cameron, R. J., M. Yu, and Y. Wang, "Direct-coupled microwave filters with single and dual stopbands," *IEEE Trans. Microw. Theory Tech.*, Vol. 53, No. 11, 3288–3297, Nov. 2005.

4. Ning, H., J. Wang, Q. Xiong, and L. Mao, "Design of planar dual and triple narrow-band bandstop filters with independently controlled stopbands and improved spurious response," *Progress In Electromagnetics Research*, Vol. 131, 259–274, 2012.

5. Gil, I., J. Garcia-Garcia, J. Bonache, F. Martin, M. Sorolla, and R. Marques, "Varactor-loaded split ring resonators for tunable notch filters at microwave frequencies," *Electron. Lett.,* Vol. 40, No. 21, 1347–1348, Oct. 2004.

6. Bouyge, D., D. Mardivirin, J. Bonache, A. Crunteanu, A. Pothier, M. Duran-Sindreu, P. Blondy, and F. Martin, "Split Ring Resonators (SRRs) based on Micro-Electro-Mechanical deflectable cantilever-type rings: Application to tunable stopband filters," *Microwave and Wireless Components Letters,* Vol. 21, No. 5, 243–245, May 2011.

7. Gil, I., F. Martin, X. Rottenberg, and W. De Raedt, "Tunable stop-band filter at Q-band based on RF-MEMS metamaterials," *Electron. Lett.,* Vol. 43, No. 21, 10, Oct. 2007.

8. Wang, X., B. Wang, H. Zhang, and K. J. Chen, "A tunable bandstop resonator based on a compact slotted ground structure," *IEEE Trans. Microw. Theory Tech.*, Vol. 55, No. 9, 1912–1917, Sep. 2007.

9. Huang, S. and Y. Lee, "A compact E-shaped patterned ground structure and its application to tunable bandstop resonator," *IEEE Trans. Microw. Theory Tech.*, Vol. 57, No. 3, 657–666, Mar. 2009.

10. Chin, K.-S. and C.-K. Lung, "Miniaturized microstrip dual-band bandstop filters using tri-section stepped-impedance resonators," *Progress In Electromagnetics Research C*, Vol. 10, 37–48, 2009.

11. Chiou, H.-K. and C.-F. Tai, "Dual-band microstrip bandstop filter using dual-mode loop resonator," *Electron. Lett.*, Vol. 45, No. 10, 507–509, 2009.

12. Vegesna, S. and M. Saed, "Microstrip dual-band bandpass and bandstop filters," *Microw. Opt. Technol. Lett.*, Vol. 54, No. 1, 168–171, 2012.

13. Huang, S. Y. and Y. H. Lee, "A compact E-shaped patterned ground structure and its applications to tunable bandstop resonator," *IEEE Trans. Microw. Theory Tech.*, Vol. 57, No. 3, 657–666, Mar. 2009.

14. Wang, J., H. Ning, Q. Xiong, M. Li, and L. Mao, "A novel miniaturized dual-band bandstop filter using dual-plane defected structures," *Progress In Electromagnetics Research*, Vol. 134, 397–417, 2013.

15. Wang, X. H., Z. Wang, H. Zhang, and K. J. Chen, "A tunable bandstop resonator based on a compact slotted ground structure," *IEEE Trans. Microw. Theory Tech.*, Vol. 55, No. 9, 1912–1918, Sep. 2007.

16. Xue, Q., K. M. Shum, and C. H. Chan, "Novel 1-D microstrip PBG cells," *IEEE Microw. Guided Wave Lett.*, Vol. 10, No. 10, 403–405, 2000.

17. Kazerooni, M., A. Cheldavi, and M. Kamarei, "A novel bandpass defected microstrip structure (DMS) filter for planar circuits," *PIERS*, 1214–1217, Moscow, Russia, Aug. 18–21, 2009.